JOURNAL OF GEOPHYSICAL RESEARCH, VOL. 105, NO. C12, PAGES 28,847–28,861, DECEMBER 15, 2000

Gravity current structure of the Chesapeake Bay outflow plume

G. O. Marmorino and C. L. Trump

Remote Sensing Division, Naval Research Laboratory, Washington, D. C.

Abstract. Measurements made across the edge of the Chesapeake Bay outflow plume in September 1996 are examined for evidence of the frontal head structure expected for a buoyant gravity current. Shipboard acoustic Doppler current profiler and hydrographic data from two distinct, 2-hour-long sets of frontal transects are analyzed. One set of observations was acquired just south of the bay mouth (near Cape Henry, Virginia) during late flood tide in water depth of 8 m. These measurements show a nearly steady frontal structure and a frontal head that is approximately 5-m deep and 20-m wide. The second data set was acquired about 20-km southeast of the bay mouth, where the plume bulges horizontally outward over the continental shelf. These measurements show a 9-m-deep frontal head (in water depth of 18 m) that ultimately dissipates during early flood tide. In both sets of observations, relative inflow of plume water into the frontal head is confined to a shallow surface layer estimated to be no more than about 2-m deep. Referenced to this layer, frontal propagation is supercritical (Froude number greater than 1). Also measured was an expected sinking motion (of the order of 3 cm/s) along the front. Overall, the results are consistent with previous measurements made across smaller buoyant plumes and in the laboratory, and they are compatible with the use of fixed values of Froude number and entrainment parameter in two-layer plume models. Additional study of the plume front during ebb tide is recommended.

1. Introduction

As relatively fresh water from a bay or river is discharged onto the continental shelf, a salinity front develops and moves outward with the current. At a distance from the source where buoyancy dominates the inertia of the discharge, the outflow detaches from the bottom and becomes a buoyant gravity current. The leading edge of a gravity current, being relatively deep, is called the "head wave" or, simply, the "head" region; and just behind the frontal head is a mixing layer into which the underlying, denser fluid is entrained and mixed with the buoyant fluid. (A schematic of the frontal head is shown in Figure 1.) Theoretical studies show that the interior flow field of the buoyant plume formed by the discharge is sensitive to assumptions made about the frontal dynamics [e.g., *Garvine*, 1987; *O'Donnell*, 1990]. This suggests that progress in modeling the plume as a whole will require a more detailed appreciation of the properties of the front.

The hydrographic structure and fluid circulation across a plume front have been measured in relatively few studies. Pioneering measurements were made by *Garvine and Monk* [1974] across the plume front formed by discharge from the Connecticut River into the Long Island Sound. This and much later work is reviewed by *O'Donnell* [1993, 1997]. *Luketina and Imberger* [1987, 1989] made a detailed study of a small-scale, radially spreading plume formed by the outflow from the Leschenault estuary into Koombana Bay, Western Australia. Their measurements, which were made at a fixed station as the front passed by, appear to show a frontal head extending to about 4-m depth (in water 10-m deep) and a region of turbulent mixing extending several hundred meters behind the surface front. New measurements of the Connecticut River plume have been reported by *O'Donnell* [1997] and *O'Donnell et al.* [1998]. In the latter work the hydrographic and velocity structure of the frontal region were measured using a near-surface array of salinity sensors and velocimeters in conjunction with a surface-deployed acoustic Doppler current profiler (ADCP). This instrumentation was deployed from a small, maneuverable boat, affording a higher spatial resolution than in previous work.

In this paper, we examine shipboard measurements similar to those of *O'Donnell et al.* [1998] but made across the edge of the plume emanating from the Chesapeake Bay (Figure 2). We will focus on measurements made in two separate study areas as indicated in Figure 2. In the inshore area, which is located 2 km southeast of Cape Henry, Virginia, a front forms as the buoyant discharge extending around Cape Henry converges with denser water found along the coast [*Marmorino et al.*, 2000]. In the offshore study area, which lies about 20 km southeast of Cape Henry, we examine the part of the plume that bulges horizontally outward over the continental shelf as part of the inertial-turning region [e.g., *Boicourt et al.*, 1987; *Chao and Boicourt*, 1986]. The front in this area has strong surface convergence as well as large across-front shear, which develops partly as the result of the Coriolis force and is an effect that is less developed in the smaller-scale plumes of the Leschenault estuary and Connecticut River.

The main objective of this paper is to investigate whether the data collected across these Chesapeake Bay outflow fronts show the structure expected of a buoyant gravity current and, in particular, whether there is evidence of a frontal head structure as in Figure 1. To provide a framework for interpreting the measurements, section 2 defines the variables of the problem. Section 3 provides background about the Chesapeake Bay field program and data selection. Sections 4 and 5 present the

Paper number 2000JC000225.

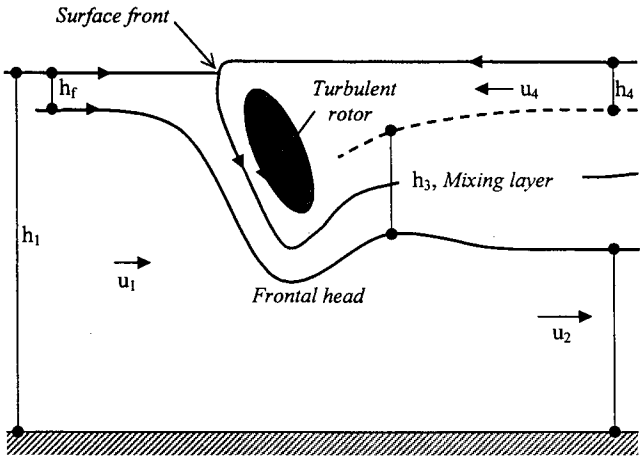

Figure 1. Schematic of circulation pattern across a plume front. See text for details. (Modified from *Luketina and Imberger* [1987, Figure 2].)

results for the inshore and offshore frontal segments. In section 6 the Chesapeake Bay results are compared with previous measurements.

2. Frontal Head

A number of important studies have been conducted on gravity currents [*O'Donnell*, 1993]. Field data have previously been compared with the laboratory experiments and analytical results of *Britter and Simpson* [1978], whose notation is illustrated in Figure 1. The independent variables of the problem include the (constant) total depth of the fluid h_1; the reduced gravity, $g' = g(\rho_1 - \rho_2)/\rho_1$, where ρ_1 is the uniform density of the ambient water, ρ_2 is the uniform density of the gravity current fluid, and g is the gravitational acceleration; and Q, which is the volume flow per unit width into the gravity current head of ρ_2 fluid. Dependent flow variables are h_4, the depth of the buoyant fluid measured well behind the head in the "tail" region of the gravity current, and u_1, the velocity of the oncoming flow required to hold the head of the gravity current steady in a fixed frame of reference or, alternatively, the frontal velocity relative to motionless ambient fluid.

The remaining variables are h_2 and u_2, the depth and velocity, respectively, of the ambient fluid beneath the gravity current; h_3 is the thickness of the mixing layer; and $u_4(Q/h_4)$ is the flow in the tail of the gravity current. In the steady state envisioned in Figure 1, mixing occurs between the plume water and the denser ambient water, so that the volume flux Q may be viewed equivalently as the flow of plume water removed from the head as a result of mixing. This requires that the average velocity in the gravity current behind the head be larger than the velocity of advance of the head. Thus u_4 may be considered as an overtaking or inflow velocity. A Froude number may be defined as $Fr \equiv u_1/(g'h_4)^{1/2}$, which gives the ratio of the frontal velocity to the phase speed in the tail of the gravity current. *Britter and Simpson*'s [1978] laboratory measurements show that the Froude number, values of which varied from about 1 to as high as 2.3, depends on the relative

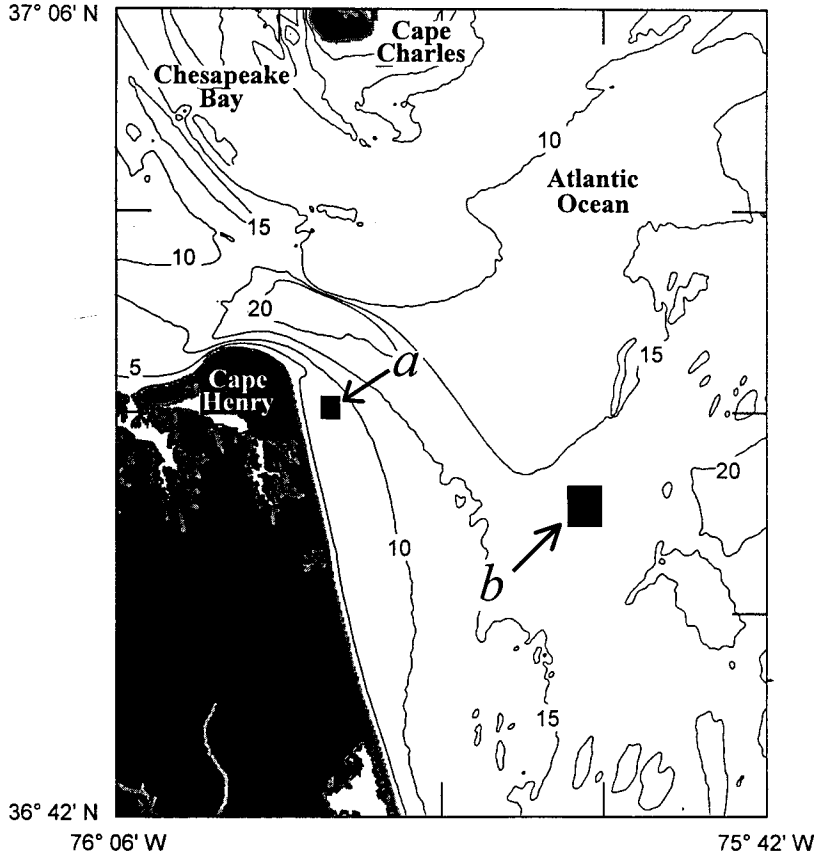

Figure 2. Location of inshore and offshore frontal studies (rectangles labeled a and b). Contours show water depth in meters.

thickness of the layers, h_4/h_1, and on the nondimensional volume flux entrained out of the gravity current at the head, $q \equiv Qg'/u_1^3$. Their experimental results and analysis were consistent with values of q in the range of 0.10 to 0.15.

The gravity current head observed by *Britter and Simpson* [1978] had the form of a wedge-shaped region with a maximum included angle with the horizontal of 40° ± 5° at the apex (which they point out is also the stagnation point in the frame of reference that holds the head stationary). Away from the apex, the interface between the two fluids was less steep and became horizontal in the tail section. Britter and Simpson also found that regular billows tended to form on the leading-edge slope of the gravity current head, rolling back under the head where they grew to large amplitude and finally breaking down into a more random velocity and salinity field that was convected away beneath the gravity current. The maximum size to which the billows grew was equal to the size of the mixed region behind the head. The billow structure was found to be quantitatively similar to the Kelvin-Helmholtz instability mechanism as their results could be explained by assuming a critical value of bulk Richardson number $Ri_{0,\text{critical}} \approx 0.35$ [*Thorpe*, 1973], where $Ri_0 \equiv g'h_3/|u_4 - u_2|^2$ was calculated from vertical differences across the mixing layer.

In *Luketina and Imberger*'s [1987, 1989] studies, vertical profiles were made at spacings of between 50 and 200 m, far too coarse to resolve the horizontal scales expected for Kelvin-Helmholtz billows, but they did measure low values of gradient Richardson number $Ri = (g/\rho)(\partial\rho/\partial z)/(\partial u/\partial z)^2$ that would be consistent with mixing induced by shear instability. These low values ($Ri < 0.3$) were found within 300 m of the surface front, corresponding to the region in Figure 1 identified as a turbulent rotor (or roller) and mixing layer. Evidence for a rotary motion in the vertical plane was identified by *Luketina and Imberger* [1987] from profiles of the horizontal velocity component. Evidence of large overturning events in these profiles suggested the generation of energetic turbulence, which decayed as the fluid advected into the more strongly stratified region downstream of the front. This was confirmed by *Luketina and Imberger* [1989], who showed that dissipation and displacement scales were high and uniform in the roller and gradually decreased through the mixing layer.

3. Chesapeake Bay Outflow Plume

3.1. Field Program

The data analyzed in this paper were collected as part of the first Chesapeake Bay Outflow Plume Experiment. This was conducted in September 1996, during which the freshwater discharge rate into the bay averaged about 4000 m^3/s (above normal for the month on account of input from two tropical storms). (For comparison, discharge rates for the Leschenault estuary and Connecticut River studies were 400 m^3/s and 1500 m^3/s, respectively.) An objective of the field program was to study the formation and evolution of the outflow plume through the use of both in situ observations and measurements made using shipboard and airborne imaging radars [e.g., *Marmorino et al.*, 1999a; *Sletten et al.*, 1999]. In situ data only are presented in this paper; all were collected aboard the University of Delaware's R/V *Cape Henlopen*.

3.2. Data Selection

Two sampling periods, both from September 25, will be analyzed in detail. These separate frontal studies were conducted in the inshore and offshore areas indicated in Figure 2. As both study areas occur away from shipping lanes (consisting of natural and dredged channels) and pilotage areas, shipboard operations were relatively unrestricted and allowed for repeated sampling. The bottom was relatively flat in each area, so no change in frontal structure is expected from local bathymetrical effects. The fronts were sampled repeatedly in a sequence of nearly normal crossings at a mean ship speed of about 1.8 (1.6) m/s for the inshore (offshore) case, care being taken to vary the crossing location so as to avoid previously disturbed water. Both cases consist of 15 realizations conducted over about a 2-hour period. Having available a large number of frontal crossings allows differentiating between sampling variability and temporally changing flow dynamics. For both sampling periods, radar data collected aboard the ship by D. Trizna were made available to us and were used to help determine frontal orientation and frontal translation rate so that the in situ velocity measurements could be put into a frame of reference fixed to the front.

3.3. In Situ Instrumentation and Data Processing

Profiles of current and acoustic backscatter intensity were measured using Towed Acoustic Doppler (TOAD) profiler [*Marmorino and Trump*, 1996]. TOAD consists of an R. D. Instruments 600-kHz ADCP suspended below a surface float. The ADCP used a vertical bin size of 0.50 m, and the shallowest bin was centered at a mean depth of 2.1 m. Mounted beneath the ADCP at a mean depth of 0.7 m was a SeaBird Instruments STD19, which recorded a value of conductivity, temperature, and pressure every 0.5 s. TOAD was deployed from a starboard outrigger and was towed at a distance of about 15 m from the side of the ship near the edge of the ship's bow-wave wake.

Additional hydrographic measurements were made using an array of four pairs of temperature and conductivity sensors suspended on a cable, which was kept taut and nearly vertical by an active depressor [*Marmorino and Trump*, 1994]. This hydrographic array was deployed from a davit located on the starboard foredeck of the ship and so was located about 15 m inboard (and about 30 m forward) of TOAD. The depth of the array was monitored using a pressure sensor mounted above the depressor. The mean depths of the sensors were 1.0, 2.1, 3.2, and 4.3 m for the inshore frontal measurements and 1.2, 2.5, 3.9, and 5.3 m for the offshore case. These data were recorded at 4 Hz and later averaged to 1-s values, giving an across-front horizontal resolution of better than 2 m. Variations in water temperature were negligible, making it convenient to use salinity S to describe the frontal hydrography. In making the salinity plots shown in sections 4.2 and 5.2, data from the hydrographic array and from TOAD were first spatially merged, taking account of the along-track offset, then numerically gridded using a combined Laplacian and spline interpolation scheme, and then contoured between the water surface and 5-m depth. Spurious or missing contours may occur near the bottom of some of the inshore sections because of shoaling of the array under higher-than-average ship speeds.

Averaging of the velocity data from the ADCP was needed to reduce noise. In order to do this while still retaining acceptable spatial resolution, the absolute position of each acoustic data bin was determined, and then the data were spatially averaged over about 10 m in the horizontal and 1 m in the vertical and then resampled at 5 m and 0.5 m. (This new procedure is described by C. L. Trump and G. O. Marmorino

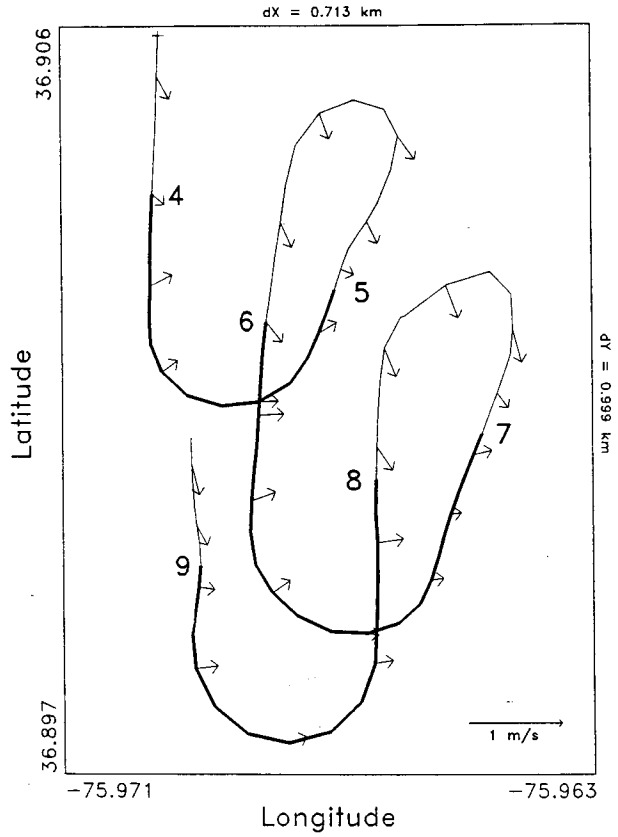

Figure 3. Subset of ship's track (0851–0922 LT) showing six consecutive crossings (4 to 9) of the inshore front. Thin (thick) track line segments indicate areas of low (high) near-surface salinity. Vectors, drawn at 1-min intervals along the track, indicate the near-surface current. Area shown is located about 2 km southeast of Cape Henry, Virginia (see rectangle "a" in Figure 2). Successive frontal crossings are offset southward, indicating southward translation of an approximately east-west oriented front.

(Resolution of small-scale frontal slope and sinking motion through spatial-registration of raw ADCP data, submitted to *Journal of Atmospheric and Oceanic Technology*, 2000), who show additional results from across the Connecticut River plume front.) The same procedure was applied to the ADCP backscatter intensity data, which are of interest because they serve to indicate qualitatively features of the frontal morphology and flow field that are unobservable in the other data. This is possible because the dominant acoustic scatterers are small (10-μm diameter) resonant bubbles that rise only slowly to the surface (at a few mm/s) and so are approximately passive tracers of the flow field. Secondary scattering may arise from turbulence-induced salinity microstructure [*Seim*, 1999]. To further reduce the effect of noise and nonfrontal signals in the ADCP data, individual across-front sections were ensemble-averaged. In portraying the results, the data were first numerically gridded and then contoured to within 1.5 m of the surface.

4. Results: Inshore Front

4.1. Sampling Overview

The inshore frontal segment was sampled from 0828 to 1028 LT, during which the wind was 5 m/s from the north-northeast. Data collection began about 2 hours after predicted maximum flood (0649 LT) and continued just beyond predicted slack water (1010 LT). (Predicted tidal stages refer to a station located in the bay mouth at 36.98°N, 76.00°W. Results from Z. R. Hallock et al. (A description of tides near the Chesapeake Bay entrance using in situ data with an adjoint model, unpublished manuscript, 1999) suggest the tidal phase at the inshore station leads that at the mouth station by about 10 min.) Thus the data span late flood through the beginning of ebb. A portion of the ship's track that includes frontal crossings 4–9 is shown in Figure 3. Thin and bold segments of the track line indicate where the ship was in either plume water ($S < 23$ psu) or ambient shelf water ($S > 28$ psu). Vectors plotted along the ship's track indicate the current at the shallowest ADCP bin. For the period shown, these currents are south southeastward at about 30 cm/s in the plume water and east northeastward at about 20 cm/s in the ambient water. The mean frontal orientation (i.e., the along-front direction) over the period of Figure 3 was 96° ± 3° T, and successive frontal crossings are offset southward as a result of a southward translation of the front.

In order to put the velocity measurements into a front-relative reference frame the across-front direction and the frontal crossing position were determined for each crossing. The crossing positions were projected onto a common across-front coordinate axis, fitted with a polynomial, and then differentiated with respect to time to yield the frontal translation velocity. The translation velocity was initially relatively small (about 14 cm/s) when the flow in the ambient water had a northward component (i.e., toward the bay mouth), but it increased to 60 cm/s over the measurement period. All reported values of the velocity component in the across-front direction have been calculated relative to the frontal translation velocity.

4.2. Hydrographic Sections

Across-front salinity sections from all 15 crossings were similar, suggesting quasi-steady frontal conditions. Five sample sections are shown in Figure 4. The data are plotted against across-front distance (x axis), measured positive toward the plume water, and with $x = 0$ corresponding to the approximate position of the surface outcrop of the front. The measurements show a steeply sloping (approximately 45°) leading edge of the frontal head. The trailing edge of the head is marked in many of the sections (e.g., Figure 4c) by a narrow region at $x \approx 25$ m where the isohalines shoal by about 1 m. Away from the head ($x > 25$ m), the isohalines are relatively flat. Stratification on the plume side of the front was strong beneath a near-surface layer of $S \approx 23$-psu water that thickened with distance from the front, reaching to about 2-m depth in some crossings at $x > 200$ m. Stratification on the ambient-water side of the front was weak initially (Figures 4a and 4b) but increased over time because of horizontal variability in the ambient water mass structure. In particular, a weak front that first appears at $x = -100$ m in Figure 4c gradually closes in on or occludes with the plume front [cf. *Marmorino et al.*, 1998]. As a consequence, the original ambient water having $S > 28$ psu submerges beneath the front (Figure 4e).

A mean salinity section computed using all but the first two crossings is shown in Figure 5. (Crossings 1 and 2 appear somewhat anomalous; see section 4.5.) On the basis of the shape of the 28.25-psu contour the mean depth of head is judged to be about 4.2 m. This is comparable to the mean depth of the deepest salinity sensor and so should be considered only a preliminary estimate of the head depth. The sur-

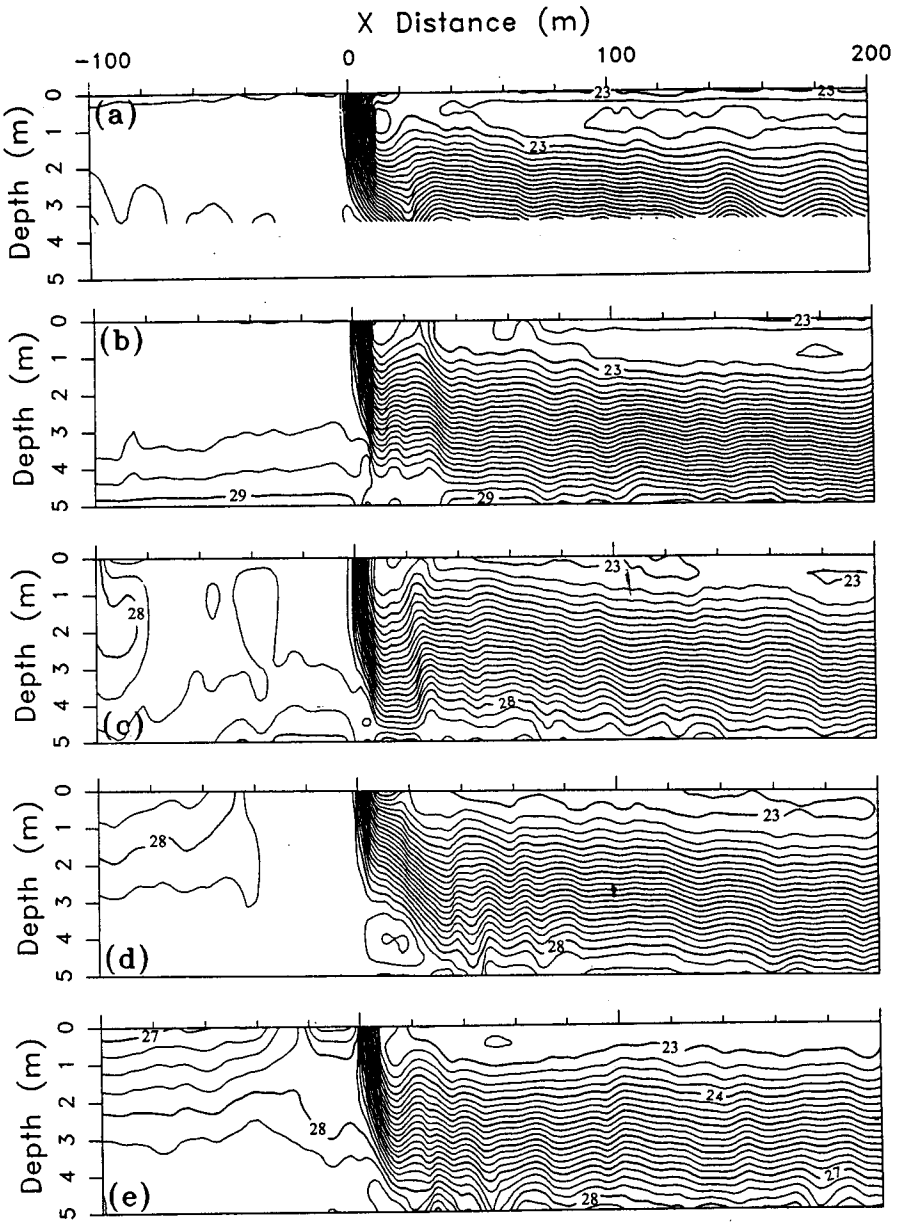

Figure 4. Across-front sections of salinity for crossings (a) 2, (b) 4, (c) 7, (d) 11, and (e) 15. Contour interval is 0.25 psu. Water depth is about 8 m. The x axis (top) shows across-front distance relative to the approximate surface outcrop of the front.

face outcrop of the 28.25-psu contour occurs at $x \approx -5$ m, while a slight shoaling of many of the isohalines occurs at $x \approx 12$ m. This gives a horizontal extent for the head of about 17 m. The horizontal-to-vertical aspect of the frontal head would thus be of the order of 4 to 1.

4.3. Mean Acoustic Backscatter Section

Figure 5b shows the vertical section of acoustic backscatter intensity averaged over the same frontal transects as for the mean salinity section. The region of the frontal head is delineated by a high-intensity core region (values as high as -76 dB) that descends steeply from the surface frontal position to a maximum depth of about 5 m. By comparison, lower and more uniform backscatter values (-100 to -102 dB) occur in the deep ambient water both ahead and beneath the plume water. Higher near-surface values occurring ahead of the front likely result from air bubbles injected by ambient breaking surface waves, while the very high backscatter values in the frontal head result from enhanced wave breaking along the front. Visual observations made at sea showed a narrow band of short and very steep "exploding" waves approximately coinciding with the salinity front and a several-meter-wide region of longer, spilling breaking waves located on the downwind side of the front. Regions such as these typically occur along convergent fronts and result from the interaction of ambient waves with the frontal surface currents [e.g., *Federov and Ginsburg*, 1992; *Lyzenga*, 1998]. Bubbles generated by the breaking waves are collected by the surface convergence and carried downward along the frontal interface and then are entrained into the frontal head. While the mean section in Figure 5b does not portray any detailed structure to the head, separate examination of single-ping backscatter data for individual acoustic

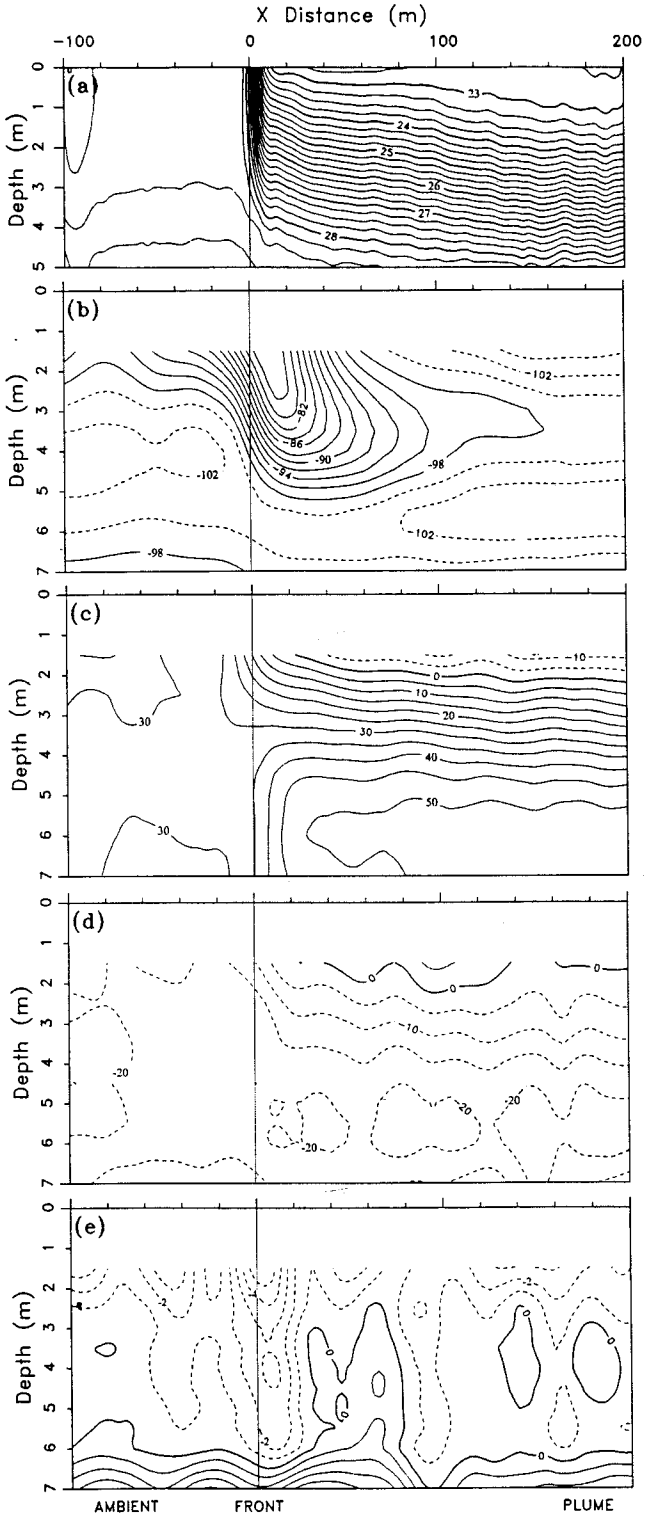

Figure 5. Ensemble-averaged sections across the inshore front. (a) Salinity. (b) Acoustic backscatter intensity (relative dB units). Solid contour lines delineate the approximate extent of water entrained into the front-head mixing layer. (c) Across-front relative velocity. (d) Along-front velocity. (e) Vertical velocity. Horizontal resolution is about 2 m (Figure 5a) and 10 m (Figures 5b–5e). Velocity units are cm/s; dashed contours (Figures 5c–5e) indicate negative values.

beams does show structure resembling a trailing edge of the head as seen in the salinity sections.

In the lee of the frontal head ($75 < x < 175$ m), high values of backscatter seem to trail away, resulting in a relative maximum in the backscatter profile at a depth of about 3 to 4 m. The pattern is consistent with gradually diminishing returns from bubbles being advected away from the head region in a mixing layer. (For a similar pattern, see *O'Donnell et al.* [1998, Figure 10].) The relative flow u_3 at a depth of 3 to 4 m is in the range of 20 to 40 cm/s (see section 4.5), so that the time for the entrained bubbles to advect 100 m horizontally is 4 to 8 min. A gradual ascent of bubbles over this time may account for an observed shoaling of the relative backscatter maximum from 4 to about 3 m.

4.4. Mean Velocity Sections

Figure 5c shows the ensemble-averaged section of across-front velocity as measured in a frame of reference translating with the front. On the ambient side of the front the relative flow is nearly uniform, so that $u_1 \approx 30$ cm/s. On the plume side of the front the 0-cm/s isotach occurs at about 2-m depth, and shallower flow of about 10 cm/s is in the negative direction. (This negative relative flow corresponds to u_4 in Figure 1.) Thus the near-surface flow approaches the front from both sides, giving an across-front current convergence of about 40 cm/s. As the width of the convergence zone is less than 40 m, the near-surface rate of convergence (or strain rate) is $\partial u/\partial x > 10^{-2}$/s. In contrast to the near surface the flow below about 4.5-m depth is divergent since the current increases across $x = 0$ m from $u_1 \approx 30$ to about $u_2 \approx 50$ cm/s. Since the vertical extent of ambient water is reduced as it passes under the plume by about a factor of 2 (i.e., from about 8 to 4 m), an increase in the velocity is to be expected. As a result, there is strong vertical shear $\partial u/\partial z$ above about 5-m depth, which is the approximate depth of the frontal head.

Figure 5d shows the average section of the along-front component of flow. Similar to the across-front component, there is uniform flow in the ambient water and strong vertical shear $\partial v/\partial z$ on the plume side of the front above about 4.5-m depth. The zero isotach ($v = 0$) lies also at about 2-m depth, so that there is no flow along the front at that depth. This is consistent with the vectors shown in Figure 3.

Figure 5e shows the average section of vertical velocity. There is a considerable amount of likely spurious signal (see below), but a narrow region centered at $x \approx 0$ m, where $w < 0$, is believed to be the expected sinking flow along the sloping frontal interface [*Garvine*, 1974; *O'Donnell et al.*, 1998]. The middepth vertical velocity $w_{z=-4\text{ m}} \approx -3$ cm/s. Figure 5e also shows a region of slightly positive w values at 30 m $< x <$ 60 m, which may be evidence of the expected upward flow near the trailing edge of the head of a gravity current [e.g., *Kao et al.*, 1977].

The vertical velocity measured at the front may be checked for consistency with the near-surface convergence by vertically integrating the continuity equation from depth $z = -D$ to the surface, $z = 0$, where $w = 0$. This yields

$$W_{z=-D} = \int_{-D}^{0} \frac{\partial u}{\partial x}\, dz,$$

where it is assumed that along-front variations are negligible. This assumption is consistent with visual observations and the available radar imagery, which showed the front as being lo-

cally straight. Using an estimate of the convergence over the upper 3 m of $\partial u/\partial x \approx -0.01$/s, one obtains $w_{z=-3\text{ m}} \approx -3$ cm/s, which is comparable to the measured value. Also, because $\partial u/\partial x$ is positive below about 3.5-m depth, the maximum sinking velocity should occur above middepth, as is observed. Because both the u and w data have been spatially smoothed, the actual sinking motion at the front may be substantially larger [e.g., see *O'Donnell et al.*, 1998, Figure 15]. Larger values would be consistent with the steeply sloping frontal interface observed in the higher-resolution salinity data.

Additional regions of ascending and descending currents also appear in Figure 5e. For example, there is a region of apparent sinking flow ahead of the front at $x \approx -50$ m. Because there is no comparable near-surface convergence $\partial u/\partial x < 0$ ahead of the front, this $w < 0$ region is assumed to be unrelated to water velocity. A speculation is that this signal arises from backscattering from organisms that sense the approaching front (possibly through the increased acoustic noise) and try to avoid it by swimming toward the bottom. Other spurious values ($w > 0$ cm/s) occur along the bottom of Figure 5e. These reflect unrealistically large values of unknown origin that occur at localized positions near the bottom in about half of the individual crossings. Likewise, an apparent sinking flow ($w < 0$ cm/s) occurs along the upper part of Figure 5e. These spurious structures should be ignored.

4.5. Temporal Evolution of Vertical Structure

The complete time history of vertical structure of some of the variables already examined in the mean is shown in Figure 6. Figure 6a shows the evolution of the salinity profile on the plume side of the front, which was constructed by averaging the profiles in each crossing over the region $50 < x < 250$ m. This range was chosen to exclude the region of the frontal head and focus on the tail of the gravity current, $x = 250$ m being the longest sample region common to all the transects. In Figure 6a, shading is used to indicate plume water having $S < 24$ psu (see below) and ambient water having $S > 28$ psu, which appears intermittently at 5-m depth. Aside from an initial period when the isohalines are deeper than average, there is relatively little change in stratification over time.

Figure 6b shows the time behavior of the tail-region backscatter profile. The most prominent feature is a band of elevated backscatter values (shown shaded in Figure 6b) lying between depths of about 2.5 and 5 m. This band is sandwiched approximately between plume and ambient water (Figure 6a) and is presumed to indicate the mixing layer. Also shown is the depth of the frontal head h_{head} (Figure 6b, circles) as estimated from the backscatter profiles averaged over $0 < x < 50$ m. Values of h_{head} lie at or just below the base of the mixing layer, as expected from *Britter and Simpson*'s [1978] experimental results. The mean head depth $\langle h_{\text{head}} \rangle = 5.1$ m (standard deviation is 0.7 m). This is a larger but possibly more realistic value than the 4.2-m depth estimated from the salinity sections.

Figure 6c shows the time behavior of the across-front flow averaged over the tail region. The maximum inflow depth, given by the depth of the $u_4 = 0$ cm/s contour, is seen to shoal over the sampling period to ~2 m from an initial depth of slightly more than 3 m. The inflow depth approximately matches that of the 24-psu salinity contour in Figure 6a. Hence water having $S < 24$ and $u_4 < 0$ cm/s is identified as plume water (shaded regions in Figures 6a and 6c). The mean thickness of the inflow layer of plume water away from the head is thus $h_4 \approx 2$ m. The initial period of deeper but shoaling contours (Figures 6a through 6c) corresponds to sample locations nearest Cape Henry; therefore a speculation is that this effect may be related to a lift-off region near Cape Henry, where buoyancy begins to dominate inertia and the plume detaches from the bottom. Also apparent in Figure 6c is the deep ambient water (shown shaded) having $u_2 > 45$ cm/s, which derives from the spatial acceleration beneath the frontal head. The mixed layer of Figure 6b lies within the high-shear (unshaded) region above the deep ambient water.

Finally, Figure 6d shows the time behavior of the relative across-front flow in the ambient water. There is an initial vertical shear that weakens over time. The weak, secondary front that was seen to develop over time in the ambient water (Figure 4) thus has an insignificant effect on the flow field.

4.6. Evolution of Frontal Parameters

The results of section 4.5 have been used to estimate the frontal Froude number $Fr = u_1/(g'h_4)^{1/2}$ for each crossing. The reduced gravity was calculated as $g' = g(\rho_1 - \rho_2)/\rho_1$, where ρ_1 is the density in the ambient water and ρ_2 is the density of the inflowing plume water at the shallowest measurement depth. In the present case, because both the near-surface plume water and the ambient water near the front are approximately homogeneous, this definition of g' is essentially identical to that used by *Britter and Simpson* [1978] (section 2). The inflow depth h_4 was estimated from the depth of the 0-cm/s isotach (Figure 6c). Uncertainty in this estimate could be as large as 1 m, leading to an error in the Froude number of the order of 25%. The ambient velocity u_1 was computed from the data in Figure 6d as a vertical average to a depth of 6 m to take account of vertical shear in the ambient water over the maximum depth extent of the frontal head. The time history of the Froude number is shown in Figure 7a. Values of Fr vary mostly between 1.1 and 1.4, exceeding unity as expected from Britter and Simpson's study. Apparent outliers having values of $Fr < 1$ occur for crossings 1, 3, and 5. Excluding these three values gives a mean Froude number $\langle Fr \rangle = 1.27$ (standard deviation is 0.08).

Similarly, Figure 7b shows a plot of the bulk Richardson number Ri_0 (section 2) calculated using data from Figure 6a and 6c between the depth of 2 and 4 m, which is the estimated depth range of the mixing layer (Figure 6b). Values of Ri_0 fall between about 0.2 and 0.5, and the mean value is $\langle Ri_0 \rangle = 0.35$ (standard deviation is 0.08). These values are consistent with those expected for shear-induced mixing (section 2). For comparison with the behavior of Fr and Ri, Figure 7c plots the frontal-head backscatter intensity I_{head}, which was determined separately for each crossing from a mean profile over the range $0 < x < 50$ m. I_{head} may be considered a qualitative indicator of frontal "strength," i.e., a measure of the combined effects of surface frontal convergence, wave breaking, bubble entrainment, turbulent microstructure, etc. Values of I_{head} fall between -62 and -73 dB, or about 30 dB above background values, with relatively little change over time.

5. Results: Offshore Front

5.1. Sampling Overview

Sampling of the offshore front was conducted from 1630 to 1830 LT. On the basis of a predicted time of 1650 LT for low-water slack in the bay mouth and a relative tidal phase lead of about 27 min, the data cover approximately the turning of the tide through early flood tide. Winds were lower (<2 m/s)

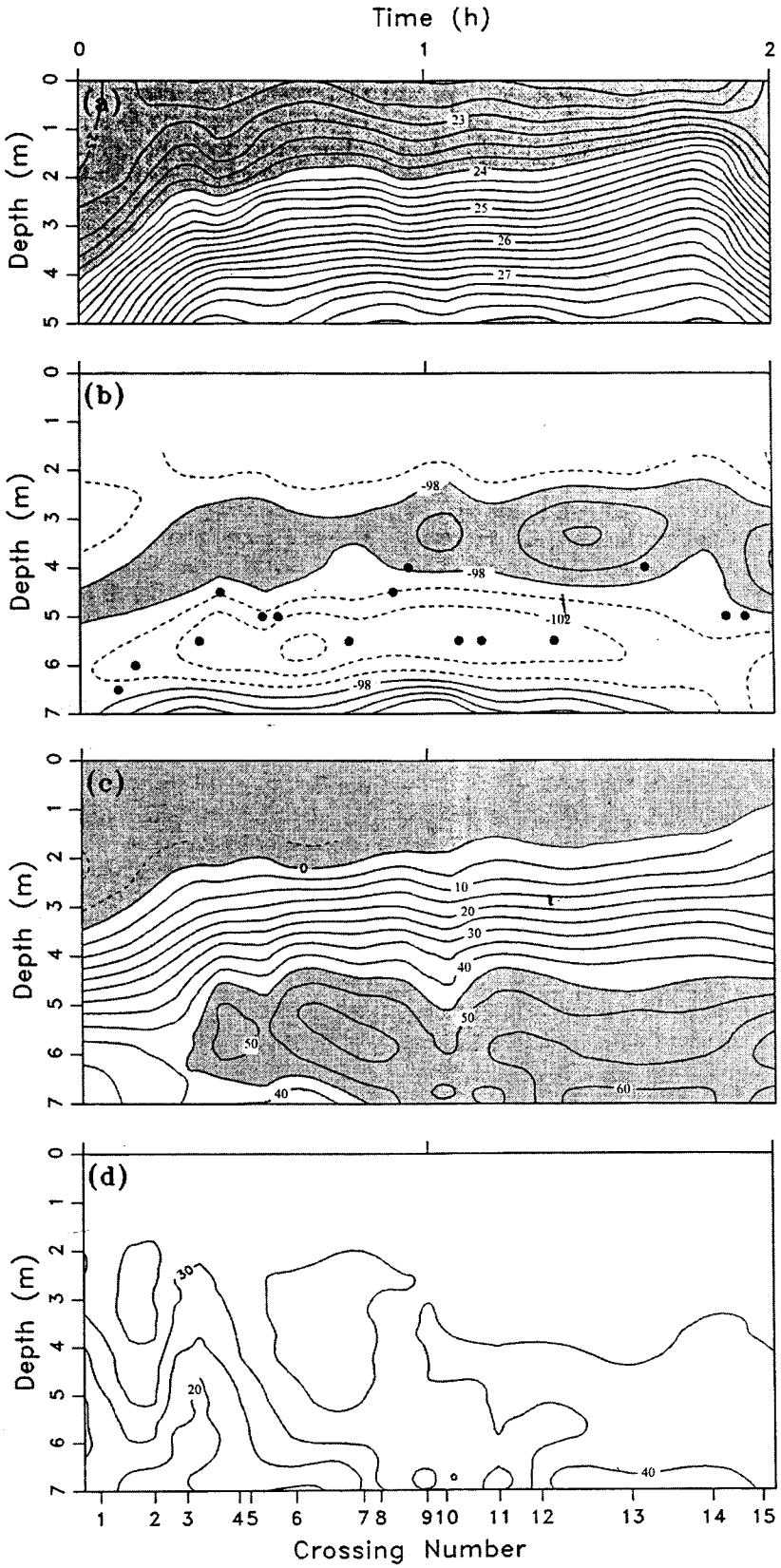

Figure 6. Time evolution of plume-side vertical structure of (a) salinity, (b) acoustic backscatter intensity, (c) across-front relative velocity, and (d) ambient-side structure of across-front relative velocity. The 2-hour period shown covers crossings 1–15 (shown at bottom) of the inshore front. For Figures 6a–6c, acoustic Doppler current profiles from each crossing were averaged over $50 < x < 250$ m, where $x = 0$ m is the frontal outcrop position; for Figure 6d, data were averaged over $-200 < x < 0$ m. Near-surface shading (Figures 6a–6c) indicates plume water (salinity <24 and relative flow toward the front), and near-bottom shading indicates undiluted ambient water (salinity > 28 psu, relative flow > 45 cm/s, and weak vertical shear $\partial u/\partial z$). In Figure 6b, shading indicates high interior values of backscatter possibly associated with the head-induced mixing layer, and circles indicate the depth of the frontal head determined separately from profiles averaged over $0 < x < 50$ m.

than for the inshore measurements made earlier in the day. The bottom depth was about 18 m. The along-front orientation was approximately constant at about 10°T. During the sampling the front moved offshore at an initial speed of 32 cm/s, decreasing to 9 cm/s for the final frontal crossing.

Results are presented in a parallel format to section 4. Thus Figure 8 shows a subset of the ship's track during the period 1648–1736 LT. Successive frontal crossings (3–10 are shown in Figure 8) are offset progressively to the east consistent with an approximately north-south front translating eastward at a mean speed of 24 cm/s for the period shown. Current vectors plotted along the ship's track indicate flow toward the south-southeast in the plume water and flow toward the north in the ambient shelf water. Ocean surface current radar (OSCR) measurements [*Haus et al.*, 1998] collected closest in time to the shipboard sampling (at 1840 UT) also show the strong across-front shear, as well as a clear anticyclonic turning of the flow emanating from the bay mouth near Cape Henry and a generally northward flow (approximately toward the bay mouth) in the ambient shelf water [*Marmorino et al.*, 1999b]. (The OSCR measurements did not cover the area of the inshore frontal study.) The occurrence of strong along-front flow makes this case less like the idealized two-dimensional gravity current than the inshore front.

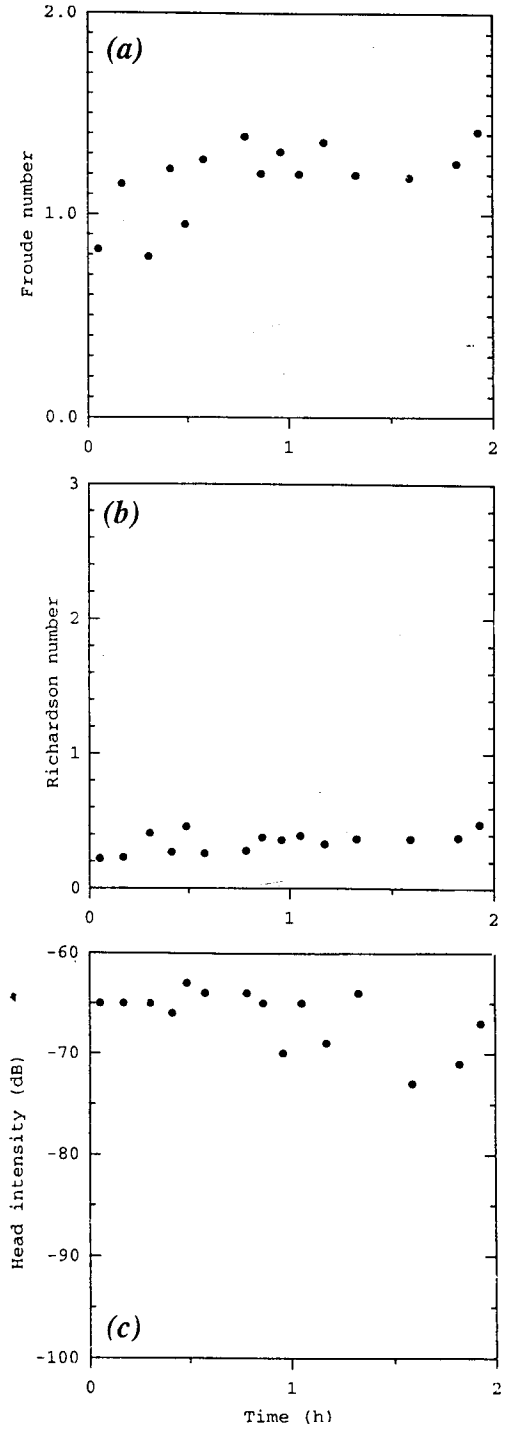

Figure 7. Evolution of characteristics for the inshore front. (a) Froude number. (b) Richardson number. (c) Head intensity.

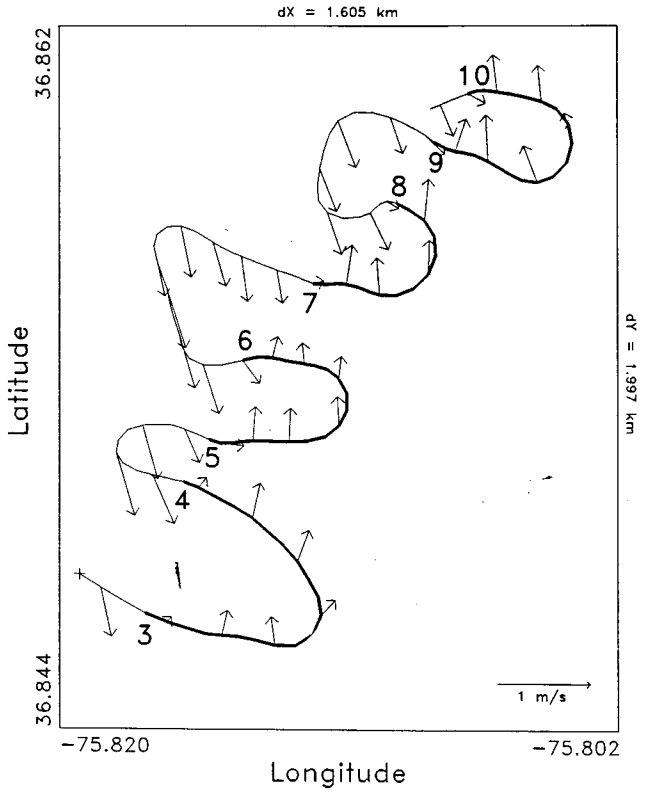

Figure 8. Subset of ship's track (1648–1736 LT) showing eight consecutive crossings (3–10) of the offshore front. Area shown is located about 20 km southeast of Cape Henry, Virginia (see rectangle "b" in Figure 2). Successive frontal crossings are offset eastward, indicating eastward translation of an approximately north-south oriented front.

5.2. Hydrographic Sections

Five sample salinity sections are shown in Figure 9. Unlike the inshore front, which showed relatively little evolution of frontal morphology, these sections show a significant weakening over time of both the near-surface horizontal salinity gradient $\partial S/\partial x$ and the stratification $\partial S/\partial z$ on the plume side of the front, so that by the time of the final crossing (Figure 9e) the frontal structure is barely distinguishable. (A weakened surface expression of the front was also evident visually at sea.) Isohalines in the leading edge of the front descend well below the depth of the hydrographic measurements. As a result, the ambient water, which has a salinity $S \geq 27$ psu, was not sampled on the plume side of the front, and the depth of the

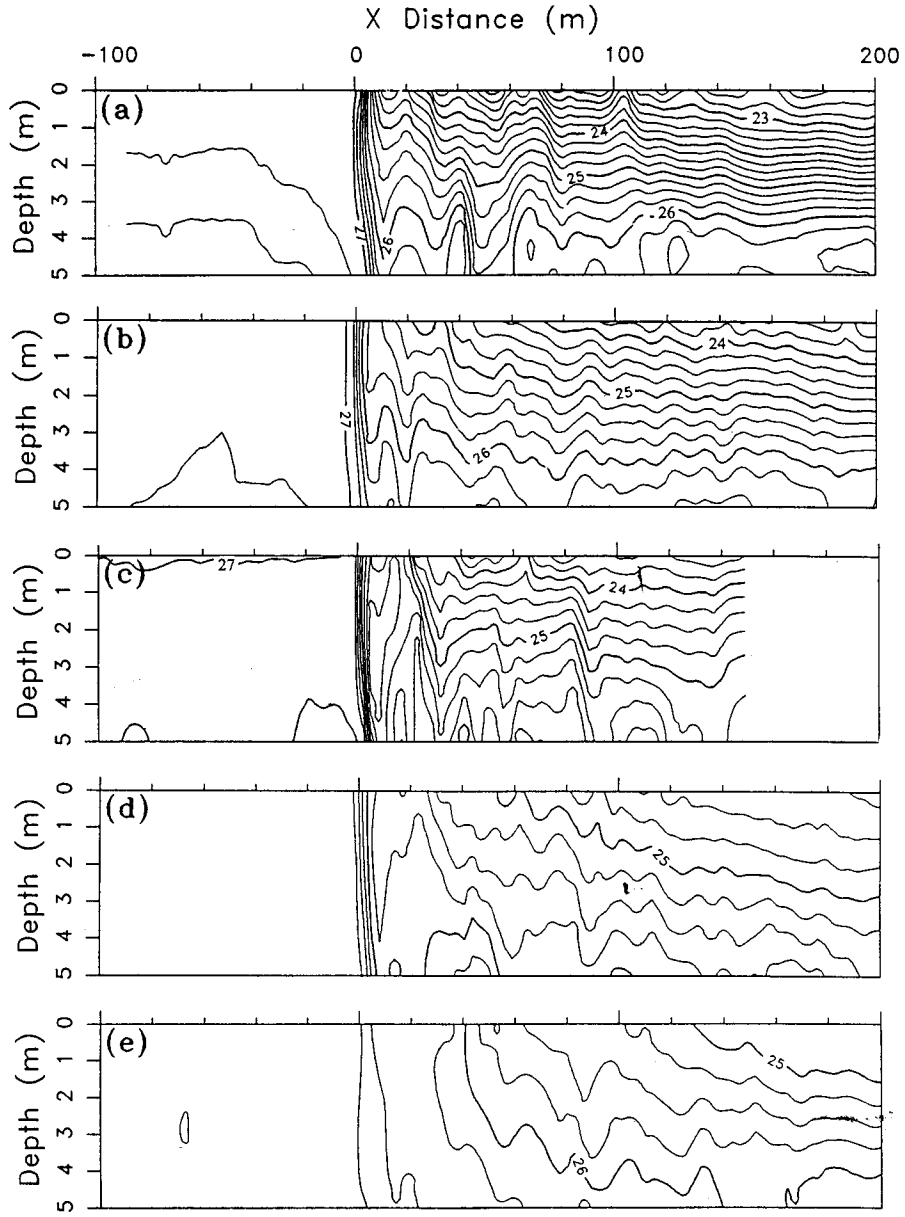

Figure 9. Across-front sections of salinity for offshore crossings (a) 1, (b) 5, (c) 8, (d) 11, and (e) 15. Water depth is about 18 m.

frontal head is indeterminate from these data. Evidence for a distinct trailing edge of the head is less clear because of the limited measurement depth and an apparently increased level of signal variability. Well behind the front, an approximately linear salinity profile extends to the surface (Figures 9a–9d), which is unlike the inshore front.

An ensemble average of the salinity data (Figure 10a) was computed over all 15 crossings. (While the frontal morphology is now clearly time-dependent, the averaging still serves to reduce noise and better elucidate a mean frontal structure.) A slight shoaling of the isohalines at $x \approx 20$ m may be taken as indicating a trailing edge of the head. The width of the frontal head is thus about 20 m, which is comparable to the head width found for the inshore front.

5.3. Acoustic Backscatter

Similar to the inshore case, the mean backscatter section (Figure 10b) shows a core region of relatively high backscatter values, which descends from the surface frontal position to a depth of (now) about 9 m. Overall, the measured backscatter values are less than for the inshore front. This would be consistent with a reduced supply of bubbles, so a likely explanation is that the lower wind speed in the afternoon resulted in a reduced spectral density of wind waves, and this resulted in less wave breaking along the front. A compounding factor may be a weaker frontal convergence as compared with the inshore front (see section 5.4). Possibly as a result of the reduced supply of bubbles, the mean data in Figure 10b now show no clear indication of a mixing layer in the lee of the head.

5.4. Velocity

The average across-front velocity section (Figure 10c) shows a near-surface frontal convergence and lower-layer divergence that is similar to but weaker in strength than the inshore front. On the ambient side, there is moderate vertical shear $\partial u/\partial z$

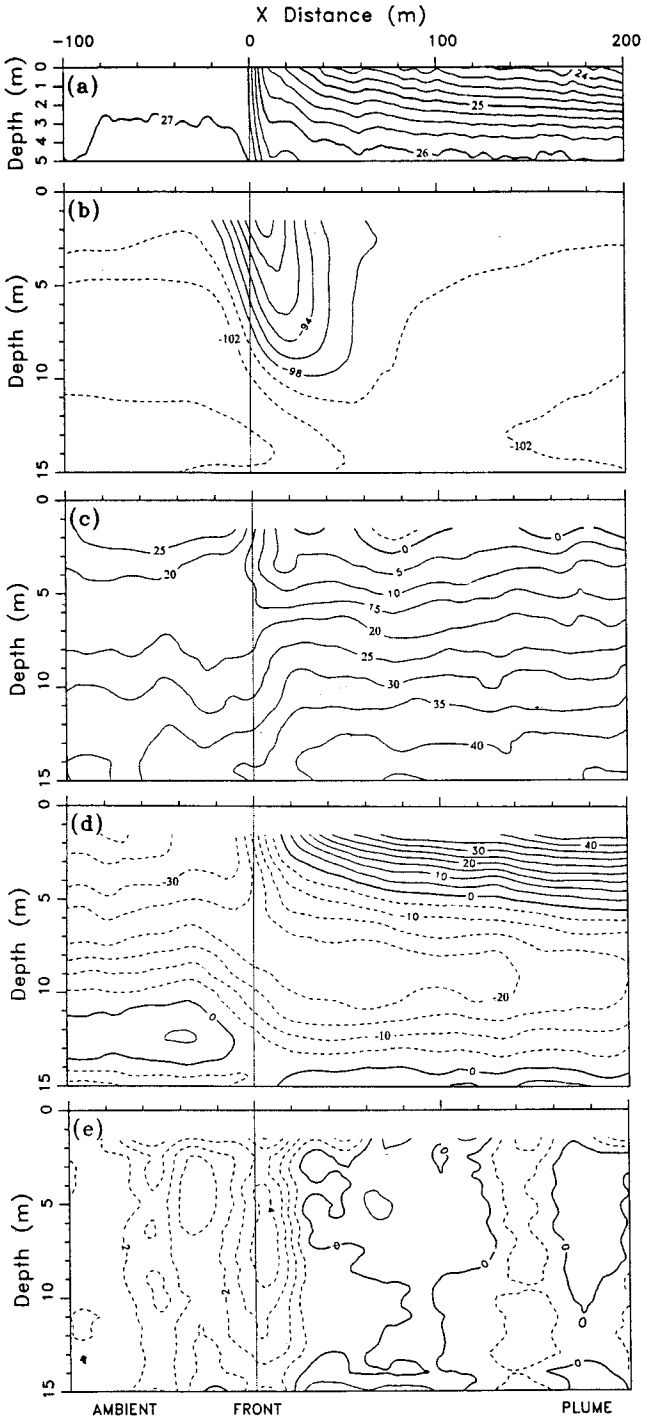

Figure 10. Ensemble-averaged sections across the offshore front. (a) Salinity. (b) Acoustic backscatter intensity. (c) Across-front relative velocity. (d) Along-front velocity. (e) Vertical velocity.

and a vertically averaged velocity of about 20 cm/s. On the plume side of the front the shear is depth-independent, and the 0-cm/s isotach again occurs at about 2-m depth, so that inflow to the frontal head occurs in a shallow layer as before.

The along-front component of flow (Figure 10d) shows the strong horizontal shear evident in the map of current vectors (Figure 8). There is strong vertical shear $\partial v/\partial z$ in the ambient water and stronger shear on the plume side of the front as the generally southward flow in the plume adjusts at depth to northward flow in the ambient water.

As for the inshore front, the section of vertical velocity (Figure 10e) shows a narrow region of sinking flow occurring at $x \approx 0$ m and a middepth value of -3 to -4 cm/s. Additional regions of ascending and descending currents also appear as for the inshore front. Missing now are the regions of spurious values along the upper and lower boundaries.

5.5. Temporal Evolution of Vertical Structure

The time history of the profiles calculated as in section 4.5 is shown in Figure 11. Shaded areas in Figures 11a and 11c indicate an approximate correspondence in depth between plume water having $S < 25$ psu and relative flow toward the front. The time evolution of the tail-region backscatter profile (Figure 11b) shows elevated values (>-98 dB, shaded region) occurring intermittently and in only the first half of the measurement period and rarely extending as deep as the frontal head (shown by the circles). Thus there is no evidence in this case of a relationship between head depth and a comparably deep head-induced mixing layer. The mean depth of the frontal head in this case is $\langle h_{\text{head}} \rangle \approx 8.7$ m (standard deviation is 1.5 m). This calculation excludes crossing 15, for which the measurements suggest a value of $h_{\text{head}} < 2$ m.

5.6. Evolution of Frontal Parameters

Figure 12 shows the time evolution of the Froude number, Richardson number, and head intensity. As in section 4.6, u_1 is calculated by vertically averaging the ambient-side front-relative flow to a depth comparable to the deepest observed head, which is taken now as 12 m. However, because of the approximately linear salinity profile on the plume side of the front, the reduced gravity is now calculated as $g' = (1/2)g(\rho_1 - \rho_2)/\rho_1$, where ρ_2 is taken as the density at 0.7-m depth on the plume side of the front. This follows the definition of g' used by *Garvine* [1974] and *O'Donnell* [1997] for the Connecticut River plume. Values of Fr are scattered between about 1.4 and 1.8. The mean value $\langle Fr \rangle = 1.62$ (standard deviation is 0.17). Two separate calculations of the Richardson number were done. The solid circles show values calculated as before, using only the u component vertical shear. These values of Ri exceed 1 and show a generally increasing trend over time, consistent with a gradually weakening frontal convergence; nevertheless, there is no corresponding trend in Froude number. Such a weakening would be consistent with a decrease in the supply of discharged water into the offshore region during early flood tide. (This is unlike the inshore front which, because of its proximity to the discharge source, forms during flood tide.) Some evidence of a weakening frontal head appears in the plot of head intensity (Figure 12c), which shows an overall decrease over time; relatively high values occur for frontal crossings 7–9, which could indicate along-front variability (see section 6.3). In the second calculation of Richardson number the total vertical shear was used, and the resulting values (Figure 12b, open circles) are uniformly low (mean value of 0.20 ± 0.04) and suggest shear-induced mixing may be occurring over the tail section despite the weakening frontal convergence.

6. Comparison With Previous Studies

6.1. Frontal Parameters

Estimates of the inshore and offshore frontal Froude number, relative layer depth h_4/h_1, and nondimensional head

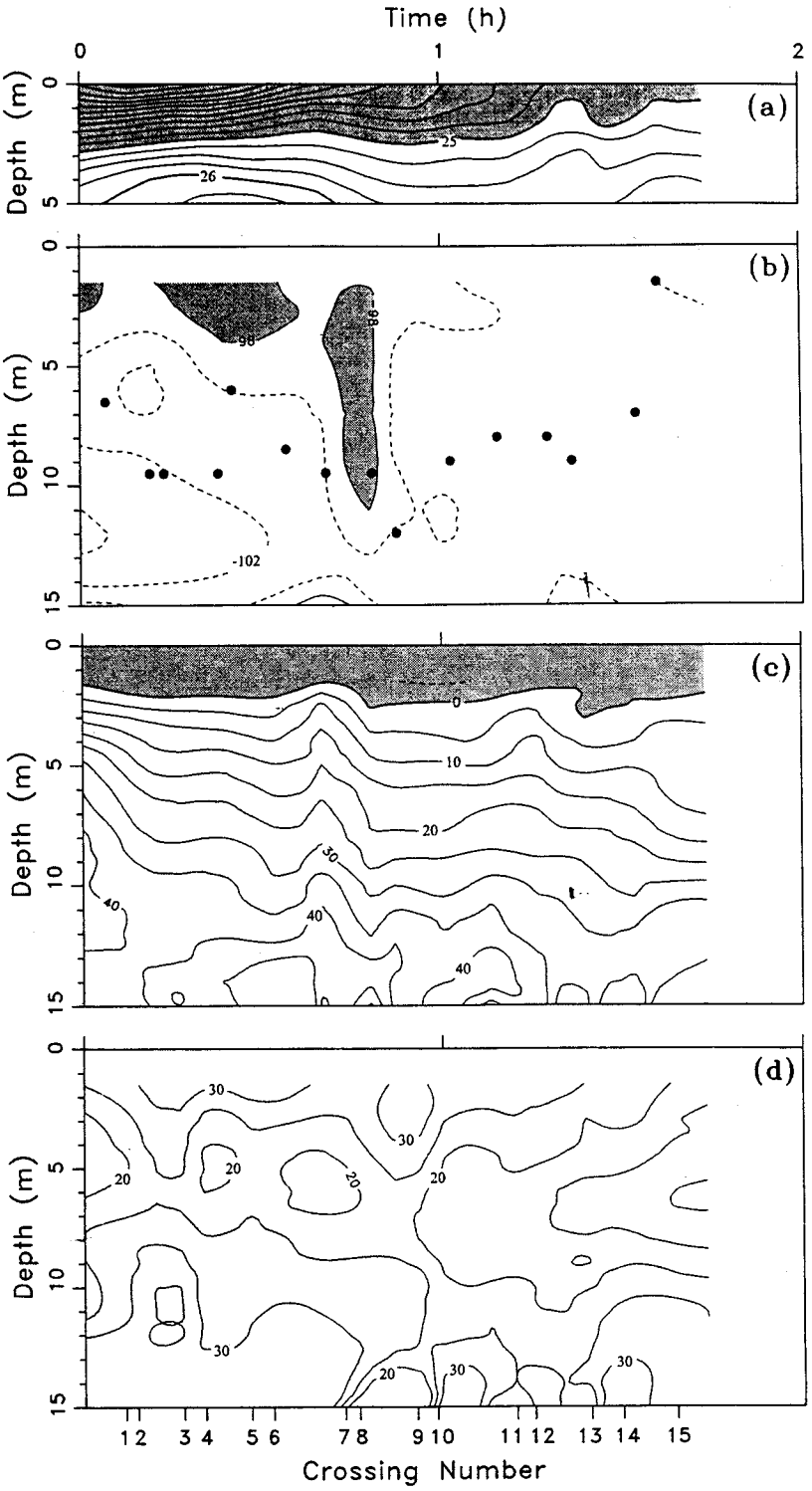

Figure 11. Time evolution of plume-side vertical structure of (a) salinity, (b) acoustic backscatter intensity (circles show depth of frontal head), (c) front-relative velocity, and (d) ambient-side structure of front-relative velocity. The 2-hour period shown covers crossings 1–15 (shown at bottom) of the offshore front.

depth h_{head}/h_1 are compared in Table 1 with results from the Leschenault estuary and Connecticut River, as well as with the laboratory measurements of *Britter and Simpson* [1978]. On the whole, the values determined for the Chesapeake Bay discharge are consistent with these previous studies. In particular, the absolute depth of the frontal head for the inshore front, $h_{\text{head}} \approx 5$ m, is comparable with the earlier studies done in similar water depth ($h_1 \approx 10$ m); and for the offshore front, where the head is nearly twice as deep, h_{head} scaled by the total water depth $h_1 \approx 18$ m is comparable to the other measurements. The depth of the inflow layer for both the inshore and offshore measurements is estimated as $h_4 \leq 2$ m. Such a shallow layer depth is also consistent with the previous field studies for which $h_4 \approx 1$ m.

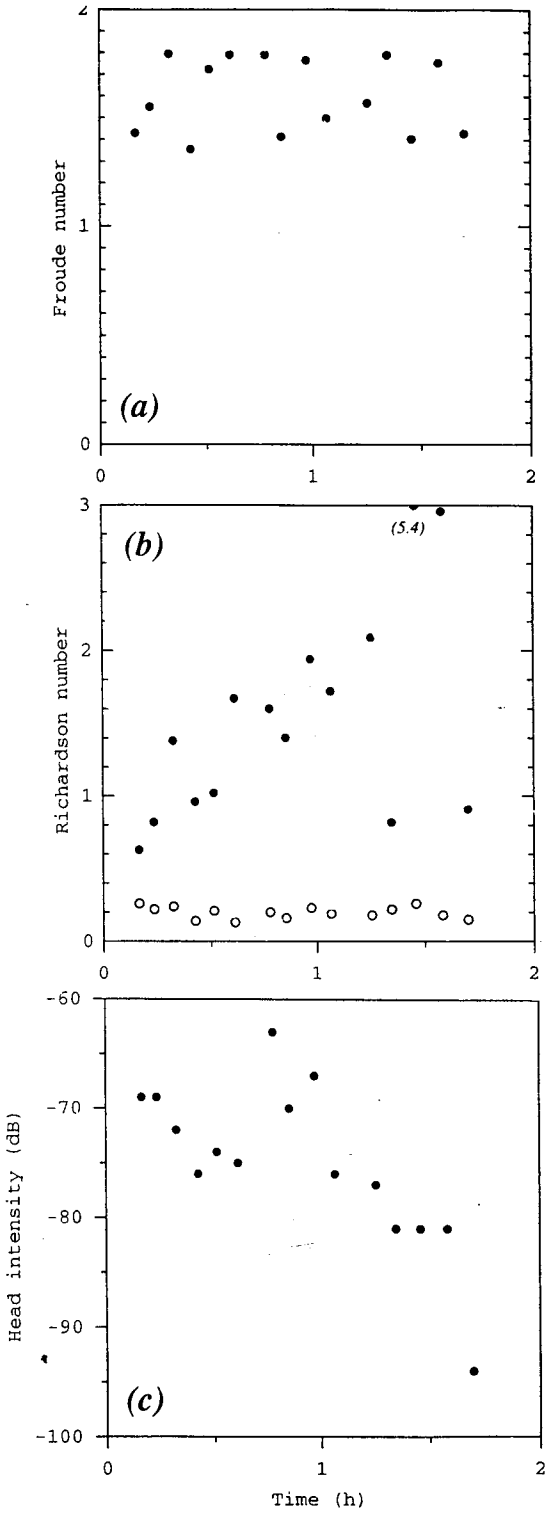

Figure 12. Evolution of offshore-front characteristics. (a) Froude number. (b) Richardson number. (c) Head intensity. The Richardson number was calculated using the across-front component of vertical shear (solid circles) and also the total vertical shear (open circles).

Perhaps, the most conspicuous result is the relatively large value $h_4/h_1 \approx 0.25$ for the inshore front. *Britter and Simpson* [1978] found that a relative depth of 0.25 represented an upper limit to the realizable value achievable in the laboratory and that for such a relatively high value of h_4/h_1 the Froude number $Fr \approx 1.2$. This compares favorably with a mean Froude number $\langle Fr \rangle \approx 1.3$ found for the inshore front. It is of interest to make a few additional estimates for the inshore front based on Britter and Simpson's results. For example, for $h_4/h_1 \approx 0.25$ and a nondimensional flux $q \approx 0.15$ (section 2), they found that the relative thickness of the mixing layer $h_3/h_4 \approx 1.5$. As we observe a value $h_4 \leq 2$ m, the expectation is that $h_3 \leq 3$ m. This compares favorably with $h_3 \approx h_{\text{head}} - h_4 \approx 3$ m near the head or $h_3 \approx 2$ m in the lee of the head (Figure 6). As another example, Britter and Simpson's expression for q may be rewritten to give $u_4 = qu_1^3/g'h_4$. Substituting the values $q \approx 0.15$, $u_1 \approx 30$ cm/s, $g' \approx 4$ cm/s^2 (a salinity difference of about 5 psu), and $h_4 \approx 200$ cm, the expected value of relative velocity into the head is $u_4 \approx 5$ cm/s. This compares with an observed value of about 5 cm/s (Figure 6c) to possibly 10 cm/s (Figure 5c). These reasonably favorable comparisons with Britter and Simpson's results add to previous evidence that the relationships they established apply at geophysical scales.

6.2. Entrainment of Ambient Water

An important feature of a gravity current is the rate of entrainment of ambient water into the overflowing stream. According to *Imberger* [1983] the volume rate of entrainment per unit frontal width $Q_p = \alpha_p u_1 h$, where α_p is the entrainment coefficient and $h = h_3 + h_4$ is the depth of the base of the turbulent mixing layer. Following *Luketina and Imberger* [1987], the entrainment coefficient may be estimated as $\alpha_p = h_f/h$, where h_f is defined as the depth of water lying ahead of the gravity current that is entrained into the mixing layer; hence h_f is the depth on the ambient side of the front of the streamline that divides the undiluted ambient water from the base of the mixing layer (see Figure 1). In the Luketina and Imberger case, $h_f \approx 2.5$ m and $h \approx 4.2$ m, giving $\alpha_p \approx 0.59$, a value they judged to apply over the leading 200 m of the gravity current.

In the case of the inshore front we propose that the acoustic backscatter measurements may be used to make a similar estimate of the entrainment coefficient. This approach assumes that the backscatter intensity is an approximately conservative tracer in the ambient water away from the regions directly affected by the surface convergence, which is a localized source of enhanced backscatter. Thus, in Figure 5b, horizontal contours lying in the deeper ambient water to the left of the front tend to extend continuously beneath the front and to become horizontal again under the plume. The shallowest such contour is the −100-dB contour, which lies at about 2.7 m on the ambient side of the front ($-100 < x < -25$ m) and between 4.5 and 5.5 m on the plume side. Water shallower than 2.7 m on the ambient side of the front and having intensities less than −100 dB is presumed to be entrained into the mixing layer; that is, we presume the −100-dB contour approximately represents the dividing streamline. This assumption was tested by using the measured two-dimensional flow field in Figures 5c and 5e to compute the path of a fluid particle initially positioned in the ambient fluid ($x = -100$ m) at a depth of 2.7 m; it was found that the fluid particle descended near the front and then leveled out at about 5-m depth if those vertical velocity data believed to be spurious were eliminated. Using the −100-dB contour as the dividing streamline, the estimate of entrainment coefficient is thus $\alpha_p = h_f/h \approx (2.7 \text{ m})/(5 \text{ m}) = 0.54$, which is comparable to *Luketina and Imberger*'s [1987] result.

Table 1. Comparison of Frontal Characteristics From Previous Field Studies of the Leschenault Estuary and Connecticut River With the Present Measurements Across the Inshore and Offshore Fronts Associated With the Chesapeake Bay Discharge and Laboratory Measurements

	Froude Number[a]	h_1, m	h_4, m	h_4/h_1	h_{head}, m	h_{head}/h_1
Leschenault estuary[b]	2.1–2.7	10	≤0.8	≤0.08	≤4	≤0.4
Connecticut River[c]	1.4–1.9	10	1	0.1	4	0.4
Inshore front	≈1.3	8	≤2	≤0.25	5	0.6
Offshore front	≈1.6	18	≤2	≤0.1	9	0.5
Laboratory[d]	1–2.3	0.1	0.01	0.1	0.05	0.4

[a]The Froude number is given by $Fr \equiv u_1/(g'h_4)^{1/2}$.
[b]See *Luketina and Imberger* [1987].
[c]See *O'Donnell et al.* [1998].
[d]See *Britter and Simpson* [1978]. In the laboratory, typical experimental values are listed for h_4 and h_{head} and values of Fr and h_{head}/h_1 are given for a relative layer depth $h_4/h_1 = 0.1$ and a nondimensional volume flux into the frontal head $q \equiv Qg'/u_1^3 = 0.15$.

6.3. Subfrontal Structure

Luketina and Imberger [1987] report the occurrence of a secondary outcropping of isopycnals at distances of 50 to 90 m behind the main front (see, in particular, their Figure 15). They attributed these "subfronts" to short-period variability in discharge strength due to seiching in the source region (i.e., the Leschenault estuary). The seiche period of the Chesapeake Bay, however, is about 1.7 days [*Boicourt et al.*, 1987], so seiching would not be expected to induce variability in the discharge over the short period of our observations; hence no subfronts should arise from this mechanism. Indeed, no subfrontal structure occurs in any of the 15 crossings of the inshore front. However, some of the offshore frontal sections do show structure resembling that found by Luketina and Imberger. An example is the section made for crossing 8 (Figure 9c), which shows an apparent subfront at $x \approx 20$ m. As this is comparable to the width of the frontal head, we speculate that such structure in the offshore front results from transient, along-front variability associated with mixing intensity.

7. Summary and Discussion

In situ measurements made across the edge of the Chesapeake Bay outflow plume have been examined for evidence of the frontal structure expected for a buoyant gravity current. Data from two distinct, 2-hour-long sets of frontal transects were analyzed. The set of observations described first was acquired just south of the bay mouth, near the Virginia coastline (in water depth of 8 m). A front tends to form close to the bay mouth (near Cape Henry) during late flood tide as the result of convergence between the buoyant outflow and ambient water that initially flows toward the bay mouth and so tends to hold the front stationary over the ground much as in *Britter and Simpson*'s [1978] laboratory experiments. The second set of measurements was made about 20 km southeast of the bay mouth (water depth of 18 m) during the early part of flood tide but while the plume front was still moving offshore. Currents and acoustic backscatter intensity were measured by using an acoustic Doppler current profiler, which was towed off to the side of a research ship, and the hydrographic structure of the frontal zone was measured over the upper 5 m of the water column by using a vertical array of sensors towed from near the bow of the ship.

In the case of the inshore front the leading edge of the frontal head was clearly delineated by a salinity interface that sloped steeply downward from the surface and curved under the plume water at a depth of nearly 5 m. The trailing edge of the frontal head was identified by a shoaling of the isohalines at a distance of about 20 m from the surface frontal outcrop. This frontal morphology appeared be relatively unchanged over the 2-hour measurement period. The frontal head also appeared as a region of enhanced acoustic backscatter. The elevated levels of backscatter are presumed to arise primarily from air bubbles that are injected at the surface through enhanced wave breaking along the front. The bubbles are then swept into the frontal interface by the convergent flow field and entrained into the head and then carried into the lee mixing region to be dispersed by shear-flow instabilities and mixed by smaller-scale turbulence. (No direct measurements were made of the fluid turbulence.) In the case of the offshore front, for which the salinity contrast and stratification are weaker and the along-front velocity component is dominant (unlike the inshore front), the measurements show a deeper frontal head but one which ultimately shrinks in size and diminishes in acoustic intensity by the end of the measurement period. In both cases, measurement of the across-front velocity field shows that inflow of plume water to the head and mixing layer is confined to a shallow layer which, though poorly resolved in these data, is estimated to be about 2 m in depth. Measurement of the vertical velocity field shows sinking at the front, and a weak ascending flow behind the frontal head, consistent with the rotor sketched in Figure 1. Estimates of the frontal Froude number, relative layer depths, bulk Richardson number, and entrainment coefficient are generally consistent with previous experimental work. Because the two distinct data sets we examined show features of consistency, we suspect the plume front will also have similar structure under a strongly ebbing tidal flow; however, such measurements have yet to be reported.

Finally, some comments on the implications of our results for the development of models of buoyant plumes are appropriate. These include both "primitive-equation" circulation-type models [e.g., *Kapolnai et al.*, 1996; *Wheless and Valle-Levinson*, 1996] and two-layer models [e.g., *Garvine*, 1987; *O'Donnell*, 1990]. The circulation model, while capable of producing a buoyant discharge and frontal region, uses a grid spacing at least an order of magnitude too large to resolve the frontal structures captured by the detailed field measurements.

Present models therefore cannot be used to investigate the effect of the front on the plume as a whole; however, the frontal physics can be resolved by appropriately embedding a high-resolution model (C. Shen, personal communication, 1999). The two-layer models, however, assume that the plume front exists and that it obeys a set of jump conditions. The frontal jump conditions require fixed bulk relationships between the ambient and plume flow and the plume layer depth D at the front. These can be expressed in terms of a constant value of Froude number $F_D \equiv u_1/(g'D)^{1/2} \approx 1.4$, where $D = h_3 + h_4$, and a constant value of an entrainment parameter $A \equiv u_4/u_1 \approx 0.2$. We estimate values of Froude number (based on h_4) that are relatively constant over time and hence consistent with the jump condition. An estimate of A for the inshore front can be made using $u_4 \approx 5$–10 cm/s and $u_1 \approx 35$ cm/s, which gives $A \approx 0.1$–0.3, and the steady state structure of the inshore front suggests A should have an approximately constant value. For the offshore front, A is similar in magnitude ($u_4/u_1 \approx$ (5 cm/s)/(20 cm/s) = 0.25), but the measurements are too imprecise to determine if it has a significantly different value because of differences in the ambient flow [*O'Donnell*, 1993]. These results are not inconsistent therefore with using a fixed value of entrainment parameter in a two-layer model. Because the two-layer models treat the front as a free boundary whose position is determined as part of the solution, additional comparisons with field data are possible. For example, *Sletten et al.* [1999] were able to make detailed maps of the Chesapeake Bay plume front as it evolved over the tidal cycle. The front contained distinct bulges and bends, many of which recurred in separate tidal cycles [*Sletten*, 1999]. An investigation into whether these frontal shapes can be reproduced using frontal jump conditions consistent with our measurements is underway [*Mied et al.*, 1999].

Acknowledgments. This paper is a contribution to the Physics of Coastal Remote Sensing Accelerated Research Initiative, which is funded by the Office of Naval Research and managed at the Naval Research Laboratory by Richard Mied. We thank the master and crew of the R/V *Cape Henlopen* for their cooperation and help in support of the field work and Dennis Trizna for access to imagery obtained from his shipboard radar system.

References

Boicourt, W. C., S.-Y. Chao, H. W. Ducklow, P. M. Glibert, T. C. Malone, M. R. Roman, L. P. Sanford, J. A. Fuhrman, C. Garside, and R. W. Garvine, Physics and microbial ecology of a buoyant estuarine plume on the continental shelf, *Eos Trans. AGU*, *68*, 666–668, 1987.

Britter, R. E., and J. E. Simpson, Experiments on the dynamics of a gravity current head, *J. Fluid Mech.*, *88*, 223–240, 1978.

Chao, S.-Y., and W. C. Boicourt, Onset of estuarine plumes, *J. Phys. Oceanogr.*, *16*, 2137–2149, 1986.

Federov, K. N., and A. I. Ginsburg, The Near-Surface Layer of the Ocean, VSP, Zeist, Netherlands, 259 pp., 1992.

Garvine, R. W., Dynamics of small-scale ocean fronts, *J. Phys. Oceanogr.*, *4*, 557–569, 1974.

Garvine, R. W., Estuary plumes and fronts in shelf waters: A layer model, *J. Phys. Oceanogr.*, *17*, 1877–1896, 1987.

Garvine, R. W., and J. D. Monk, Frontal structure of a river plume, *J. Geophys. Res.*, *79*, 2251–2259, 1974.

Haus, B. K., H. C. Graber, L. K. Shay, S. Nikolic, and J. Martinez, Ocean surface current observations with HF Doppler radar during the Chesapeake Bay Outflow Plume Experiment (COPE-1), *Tech. Rep. RSMAS 98-003*, Rosenthiel Sch. of Mar. and Atmos. Sci., Univ. of Miami, Miami, Fla., 1998.

Imberger, J., Tidal jet frontogenesis, *Mech. Eng. Trans. Inst. Eng. Aust.*, *8*, 171–180, 1983.

Kao, T. W., C. Park, and H.-P. Pao, Buoyant surface discharge and small-scale oceanic fronts: A numerical study, *J. Geophys. Res.*, *82*, 1747–1752, 1977.

Kapolnai, A., F. E. Werner, and J. O. Blanton, Circulation, mixing and exchange processes in the vicinity of tidal inlets: A numerical study, *J. Geophys. Res.*, *101*, 14,253–14,268, 1996.

Luketina, D. A., and J. Imberger, Characteristics of a surface buoyant jet, *J. Geophys. Res.*, *92*, 5435–5447, 1987.

Luketina, D. A., and J. Imberger, Turbulence and entrainment in a buoyant surface plume, *J. Geophys. Res.*, *94*, 12,619–12,636, 1989.

Lyzenga, D. R., Effects of intermediate-scale waves on radar signatures of ocean fronts and internal waves, *J. Geophys. Res.*, *103*, 18,759–18,768, 1998.

Marmorino, G. O., and C. L. Trump, A salinity front and current rip near Cape Hatteras, North Carolina, *J. Geophys. Res.*, *99*, 7627–7637, 1994.

Marmorino, G. O., and C. L. Trump, High-resolution measurements made across a tidal intrusion front, *J. Geophys. Res.*, *101*, 25,661–25,674, 1996.

Marmorino, G. O., C. Y. Shen, N. Alan, F. Askari, D. B. Trizna, C. L. Trump, and L. K. Shay, An occluded oceanic front, *J. Geophys. Res.*, *103*, 21,587–21,600, 1998.

Marmorino, G. O., C. L. Trump, and D. B. Trizna, Preliminary observation of a tidal intrusion front inside the mouth of the Chesapeake Bay, *Estuaries*, *22*, 105–112, 1999a.

Marmorino, G. O., L. K. Shay, B. K. Haus, R. A. Handler, H. C. Graber, and M. P. Horne, An EOF analysis of HF Doppler radar current measurements of the Chesapeake Bay buoyant outflow, *Cont. Shelf Res.*, *19*, 271–288, 1999b.

Marmorino, G. O., T. F. Donato, M. A. Sletten, and C. L. Trump, Observations of an inshore front associated with the Chesapeake Bay outflow plume, *Cont. Shelf Res.*, *20*, 665–684, 2000.

Mied, R. P., A. L. Cooper, and G. J. Lindemann, Modeling studies of the frontal evolution of buoyant plumes (abstract), *Eos Trans. AGU*, *80*(49), Ocean Sci. Meet. Suppl., OS182, 1999.

O'Donnell, J., The formation and fate of a river plume: A numerical model, *J. Phys. Oceanogr.*, *20*, 551–559, 1990.

O'Donnell, J., Surface fronts in estuaries: A review, *Estuaries*, *16*, 12–39, 1993.

O'Donnell, J., Observations of near-surface currents and hydrography in the Connecticut River plume with the surface current and density array, *J. Geophys. Res.*, *102*, 25,021–25,033, 1997.

O'Donnell, J., G. O. Marmorino, and C. L. Trump, Convergence and downwelling at a river plume front, *J. Phys. Oceanogr.*, *28*, 1481–1495, 1998.

Seim, H. E., Acoustic backscatter from salinity microstructure, *J. Atmos. Oceanic Technol.*, *16*, 1491–1498, 1999.

Sletten, M. A., A comparison of the Chesapeake Bay outflow plume front evolution as observed with a real aperture radar during COPE2 and COPE5 (abstract), *Eos Trans. AGU*, *80*(49), Ocean Sci. Meet. Suppl., OS182, 1999.

Sletten, M. A., G. O. Marmorino, T. F. Donato, D. J. McLaughlin, and E. Twarog, An airborne, real aperture radar study of the Chesapeake Bay outflow plume, *J. Geophys. Res.*, *104*, 1211–1222, 1999.

Thorpe, S. A., Experiments on instability and turbulence in a stratified shear flow, *J. Fluid Mech.*, *64*, 731–751, 1973.

Wheless, G. H., and A. Valle-Levinson, A modeling study of tidally driven estuarine exchange through a narrow inlet onto a sloping shelf, *J. Geophys. Res.*, *101*, 25,675–25,687, 1996.

G. O. Marmorino and C. L. Trump, Remote Sensing Division, Naval Research Laboratory, Code 7250, 4550 Overlook Avenue SW, Building 2-B, Room 108, Washington, DC 20375-5351. (marmorino@nrl.navy.mil)

(Received January 14, 2000; revised June 27, 2000; accepted August 9, 2000.)